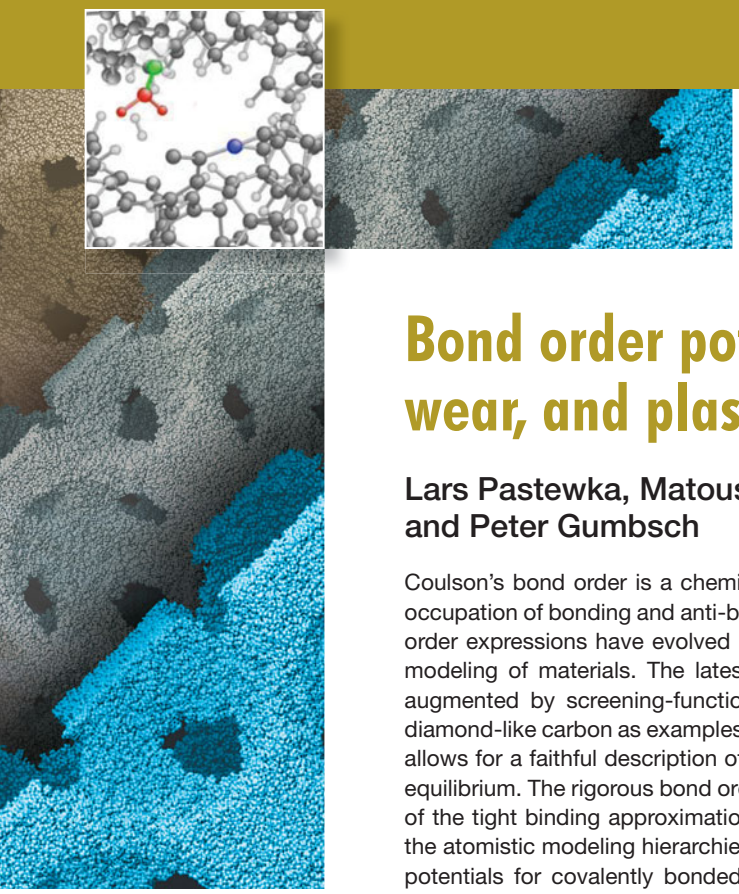


Bond order potentials for fracture, wear, and plasticity

Lars Pastewka, Matous Mrovec, Michael Moseler, and Peter Gumbsch

Coulson's bond order is a chemically intuitive quantity that measures the difference in the occupation of bonding and anti-bonding orbitals. Both empirical and rigorously derived bond order expressions have evolved in the course of time and proven very useful for atomistic modeling of materials. The latest generation of empirical formulations has recently been augmented by screening-function approaches. Using friction and wear of diamond and diamond-like carbon as examples, we demonstrate that such a screened bond order scheme allows for a faithful description of dynamical bond-breaking processes in materials far from equilibrium. The rigorous bond order expansions are obtained by systematic coarse-graining of the tight binding approximation and form a bridge between the electronic structure and the atomistic modeling hierarchies. They have enabled bottom-up derivations of bond order potentials for covalently bonded semiconductors, transition metals, and multicomponent intermetallics. The recently developed magnetic bond order potential gives a correct description of both directional covalent bonds and magnetic interactions in iron and is able to correctly predict the stability of bulk Fe polymorphs as well as the intricate properties of dislocation cores. The bond order schemes hence represent a family of reliable and powerful models that can be applied in large-scale simulations of complex processes involving fracture, wear, and plasticity.

Introduction

A quantitative microscopic understanding of the behavior of real materials under realistic conditions still presents a great challenge for atomic-scale modeling. Especially challenging are simulations of processes involving plastic deformation, fracture, wear, thin-film growth, or ion-beam etching, since they require an accurate description of strongly distorted atomic configurations with rapidly changing bonding conditions in large atomic ensembles containing thousands or even millions of atoms. Interatomic potentials suitable for description of such complex processes therefore must be both computationally efficient and reliable in the description of interatomic interactions.

One of the most successful families of interatomic potentials that has been able to stand the demanding requirement of simultaneous efficiency and reliability is the family of models based on the quantum-mechanical concept of bond order, introduced by Coulson[1] long before the advent of atomistic simulations. In the intuitive language of chemical molecular orbital theory, the bond order simply characterizes the strength of a chemical bond, since it corresponds to one-half of the difference between the number of electrons in the bonding and anti-bonding states. In the elementary H_2 molecule, the bond order is equal to one since the bonding state is fully occupied by two electrons with opposite spins, while the anti-bonding state remains empty. In more complicated molecules or in solids, the bonds are usually not fully saturated due to the influence of the atomic environment, and, as a result, their bond orders are less than unified.

A more rigorous, quantitative definition of the bond order requires an introduction of some basic quantum mechanical terminology. The usual way to solve the one-particle Schrödinger equation

$$\hat{H}|n\rangle = \varepsilon^{(n)}|n\rangle, \qquad (1)$$

where $\hat{H}$ is the Hamiltonian operator, $|n\rangle$ are the single-particle eigenfunctions, and $\varepsilon^{(n)}$ the corresponding eigenvalues, is to

Lars Pastewka, Fraunhofer Institute for Mechanics of Materials IWM and Institute for Applied Materials IAM at Karlsruhe Institute of Technology, Germany; lars.pastewka@iwm.fraunhofer.de
Matous Mrovec, Fraunhofer Institute for Mechanics of Materials IWM and Institute for Applied Materials IAM at Karlsruhe Institute of Technology, Germany; matous.mrovec@kit.edu
Michael Moseler, Fraunhofer Institute for Mechanics of Materials IWM and Physics Department of the University of Freiburg, Germany; michael.moseler@iwm.fraunhofer.de
Peter Gumbsch, Fraunhofer Institute for Mechanics of Materials IWM and Institute for Applied Materials IAM at Karlsruhe Institute of Technology, Germany; peter.gumbsch@kit.edu
DOI: 10.1557/mrs.2012.94

© 2012 Materials Research Society

https://doi.org/10.1557/mrs.2012.94 Published online by Cambridge University Press

convert it into a matrix eigenvalue problem. Following the chemically intuitive tight-binding (TB) model,[2,3] the eigenfunctions are expanded into a minimal set of localized atomic-like orbitals

$$|n\rangle = \sum_{i\alpha} C_{i\alpha}^{(n)} |i\alpha\rangle, \tag{2}$$

where i is a site index, α is an orbital index, and $C_{i\alpha}^{(n)} \equiv \langle i\alpha|n\rangle$ is the expansion coefficient of orbital $i\alpha$. It is assumed here for simplicity that the atomic-like orbitals $|i\alpha\rangle$ are real and orthonormal. Combining Equations 1 and 2 obtains the secular equation

$$\sum_{j\beta} H_{i\alpha,j\beta} C_{j\beta}^{(n)} = \varepsilon^{(n)} C_{i\alpha}^{(n)}, \tag{3}$$

where the Hamiltonian operator is now expressed in the matrix form as $H_{i\alpha,j\beta} = \langle i\alpha|\hat{H}|j\beta\rangle$ for orbitals $i\alpha$ and $j\beta$. Using the well-known two-center parameterization of Slater and Koster,[4] the inter-site elements $H_{i\alpha,j\beta}$ can be expressed directly in terms of distance-dependent two-center integrals, which are also known as bond or hopping integrals. Typically, in semi-empirical TB approaches, the bond integrals are treated as fixed functions whose parameters are obtained by fitting to more accurate electronic structure calculations. The parameterization of the Hamiltonian matrix elements as functions of the atomic positions, which will be addressed later, is the most critical part of any TB model.

Using the previous notation, the bond order between orbitals $|i\alpha\rangle$ and $|j\beta\rangle$ is then given as

$$\Theta_{i\alpha,j\beta} = 2\sum_{n(\mathrm{occ})} C_{i\alpha}^{(n)} C_{j\beta}^{(n)} = 2\rho_{i\alpha,j\beta} \qquad (i\alpha \neq j\beta), \tag{4}$$

where $\rho_{i\alpha,j\beta}$ are off-diagonal elements of the density matrix—a quantity known more commonly among the solid-state physics community. The sum runs over all occupied eigenfunctions n(occ). The factor of two accounts for spin degeneracy, but more general spin-unpaired formulations also exist.[3]

Equation 4 presents a rigorous definition of the bond order within the TB theory. It enables expression of the total bond energy associated with the formation of chemical bonds as a sum over individual bonds

$$E_{\mathrm{bond}} = \sum_{i\alpha \neq j\beta} \Theta_{j\beta,i\alpha} H_{i\alpha,j\beta}. \tag{5}$$

This deceptively simple equation is the defining equation for all bond order schemes. It shows that the strength of bonding is given as the product of pairwise bond integrals, which need to be parameterized, and bond orders, which need to be calculated. The major complication hidden in Equation 5 is that the bond orders are not pairwise quantities, but they generally depend on the positions of all atoms in the system. In standard TB approaches, the bond orders in Equation 4 are obtained by solving the secular Equation 3 by matrix diagonalization. However, this mathematical procedure is impractical for large systems, since its computational cost scales with the cube of the number of atoms, limiting the accessible size of the system under study to a few hundred atoms. The key idea of all classical interatomic potentials is to avoid the non-local solution and to express instead the bond order in Equation 5 via a short-ranged function of the positions of the neighboring atoms only. Naturally, the main reason for such a direct formulation is to gain a significant speed-up of the calculations, ideally reaching the linear scaling necessary for large-scale molecular dynamics simulations. However, it must not be forgotten that every local expression is an approximation to the exact TB solution based on the assumption that the strength of a chemical bond is mainly influenced by its local environment.

Many-body expansions

Although the theoretical basis is not as firm as for potentials based, for example, on effective medium theory, expansions of the potential energy as sums of pairs and triplets of atoms are commonly used as potential energy functions. The most widely used form is the valence force field in which covalent bonding is modeled as a harmonic expansion in bond stretches, bends, dihedral rotations, and combinations of stretches and bends, with the force constants typically fit to structures and vibrational frequencies. These harmonic expansions are usually supplemented with longer-ranged interactions involving electrostatic terms and relatively weak non-bonded forces.

As detailed by Finnis in this issue, there are two ways to construct an interatomic potential. The first way is the artistic route of empirical design using chemical and physical insights together with convenient functional forms. The second alternative is the rigorous approach of a bottom-up derivation of the functional forms from a higher level theory, in our case TB. Both of these procedures have been applied in the construction of bond order expressions, and both approaches turned out to be largely successful. This success can be likely attributed to the general validity of the fundamental Equation 5. In this article, we provide an overview of many-body potentials constructed by following both routes—the artistic route of empirical design and the rigorous route of bottom-up derivation. Both routes have their virtues and their weaknesses, but, more importantly, it will be shown that they do not diverge but rather seem to approach each other.

Before going into details, it must not be forgotten that the total binding or cohesive energy of an atomic ensemble is not equal just to the sum of individual bond energies. In addition to this major attractive contribution, there are other terms that

https://doi.org/10.1557/mrs.2012.94 Published online by Cambridge University Press

depend on the material under study and its bonding character. In a general case, the total binding energy E_B can be written as

$$E_B = E_{bond} + E_{rep} + E_{prom} + E_{mag} + E_{ion} + E_{vdW}, \quad (6)$$

where E_{rep} is a repulsive energy arising from the overlap and electrostatic repulsion of the atoms, E_{prom} is the promotion energy reflecting the change of the hybridization state on bonded atoms with respect to their atomic ground states, E_{mag} is the magnetic energy contribution associated with the formation of magnetic moments on atoms, E_{ion} is the ionic energy in polar bonding environments where there is a net charge transfer between the atoms, and E_{vdW} is the weak van der Waals contribution. The majority of the models described here deal with dense covalent and metallic materials, in which the last two contributions in Equation 6 can be neglected. Thus, in this article, the ionic and van der Waals bonding are excluded hereafter.

In addition to describing the underlying concepts of various bond order schemes, we will present several applications from our own studies on tribology and plasticity in order to demonstrate the robustness and predictive power as well as the limitations of existing models.

Abell-Tersoff-Brenner: Empirical formulations for the bond order

The history of empirical bond order schemes is usually thought to start with the work of Abell,[5] who suggested an expression of the universal binding energy relations in solids using a bond order function. Soon after Abell, Tersoff proposed an explicit expression for the bond order and applied it to silicon.[6] The resulting interatomic potential turned out to be remarkably transferable to a wide range of silicon allotropes and was later parameterized also for carbon and silicon-carbon interactions.[7]

In Tersoff's potential, the bond and repulsive energy are given, respectively, as

$$E_{bond} = -\sum_{i,j\neq j} \Theta_{ji} h_{ij} \quad \text{and} \quad E_{rep} = \sum_{i,j\neq j} V_{ij}. \quad (7)$$

Both the bond integral h_{ij} and the repulsive potential V_{ij} are pairwise functions that depend on the interatomic distance R_{ij} between the atoms i and j only and are required to become zero before the second-neighbor shell in the ground-state crystalline structure. In contrast, the expression for the bond order is a many-body function, which contains both distance and angular dependent terms. Despite its empirical nature, Tersoff's expression for the bond order[8] has been shown to be extraordinarily flexible and has been used to construct interatomic potentials for a number of systems (e.g., Al-N,[9] B-C-N,[10–12] C-O,[13] Fe-C,[14,15] Si-C,[6,7,16] W-C,[17] Ga-As,[18] and Zn-O).[19]

A few years after Tersoff's initial work, Brenner presented a parameterization for hydrocarbons, which was later named as the reactive empirical bond order (REBO) potential.[20,21] Brenner realized that Tersoff's initial functional form was too simplistic to describe the wide variety of bonding situations and the complex chemistry found in hydrocarbons. He proposed to correct the potential based on look-up tables whose entries were selected by the coordination numbers N_i and an additional variable N_{ij}^{conj} describing the conjugation state of bond i–j. The set of numbers $\{N_i, N_j, N_{ij}^{conj}\}$ can be regarded as a fingerprint of the local chemical environment that reaches out to second-nearest neighbors, making the potential effectively longer-ranged than that of Tersoff. The second-generation of Brenner's potentials (REBO2),[22] published about 10 years later, further improved the description of crystalline bulk phases and π-bonded molecules by modifying the conjugation parameter N_{ij}^{conj} and by adding a dihedral energy contribution that penalizes the rotation of adjacent hydrocarbon groups, such as the C–C bond rotation in ethylene. Another extension of the REBO formalism[23] included an expression for E_{vdW} for modeling of the liquid and vapor phases in which non-bonded interactions become important.

The REBO potentials enabled the study of carbon in a broad range of bonding environments (e.g., diamond, graphite, fullerenes, nanotubes, simple polymers, diamond-like carbon, carbynes) and processes involving subtle structural variations. One of the first successes of the original REBO was the prediction of the dimer opening process on the (001) (2 × 1) diamond surface that was believed to play a crucial role in the chemical vapor deposition growth of diamond.[24] Since then, the family of Abell-Tersoff-Brenner (ATB) potentials has been used extensively in simulations of vapor deposition processes of diamond[25] and amorphous carbon (a-C),[26,27] irradiation damage in silicon,[28] friction of polymers,[29] mechanical properties of carbon nanotubes,[30] and graphene,[31] to name a few examples.

Despite these numerous successes, ATB potentials have been known to fail under certain circumstances. One of the most apparent failures occurs when the bonds are significantly stretched beyond their equilibrium distances, for instance, under large external loads or in the vicinity of the crack tip.[32] **Figure 1**a shows a crack tip in diamond simulated with REBO2. Instead of crack tip propagation, as expected for a brittle material, the potential predicts the crack to emit dislocations and blunt. A similar failure of the REBOs is observed for the fracture of carbon nanotubes and graphene.[33]

It is important to stress that this unphysical behavior does not imply the failure of the bond order concept. It simply originates from the applied fitting scheme that assumes that the bond integral $h(R)$ and the repulsive potential $V(R)$ are rather short ranged in order to minimize the computational load.[33] This "shortsightedness" is enforced by multiplying the asymptotic $h_0(R)$ and $V_0(R)$ with a cutoff function $f_C(R)$ that drops from unity to zero between first- and second-nearest neighbors in the equilibrium diamond structure. Figure 1c–d shows the effect of the cutoff function (shown in Figure 1e–f) on the energetics of a carbon dimer. A steep drop in the energy enforced by f_C leads to a peak in the force that is substantially larger than the force from the potential without cutoff.[34] This overestimation favors dislocation nucleation over brittle fracture in crystalline carbon allotropes.[33]

A common cure for the force overestimation problem is the truncation of forces instead of energies. It was first used in studies on fracture of polycrystalline diamond[35] and later

https://doi.org/10.1557/mrs.2012.94 Published online by Cambridge University Press

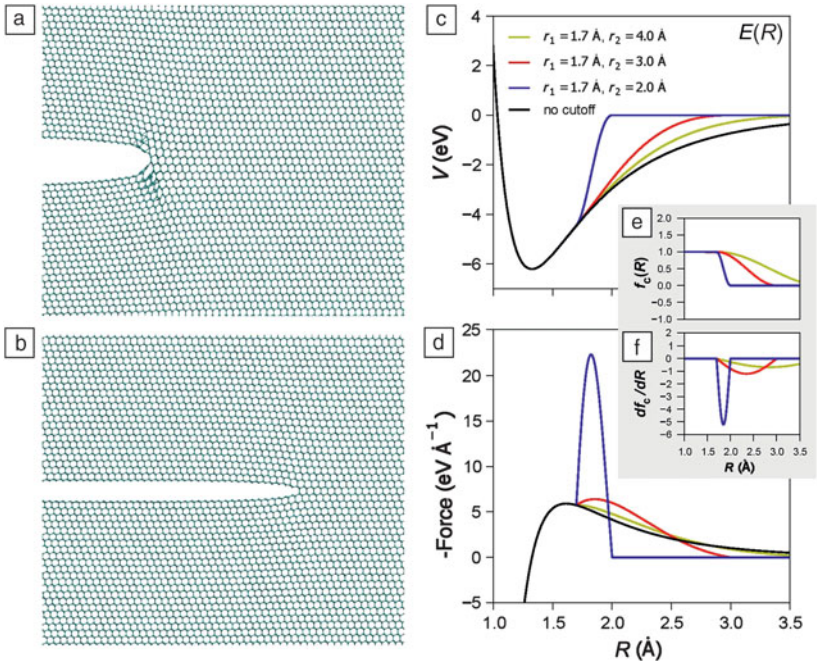


Figure 1. Panels (a) and (b) show examples where REBO2 gives unphysical behavior that is cured by using REBO2+S. In a dynamic simulation, a crack in diamond blunts (a), but propagates (b) at identical strain in REBO2+S. Panels (c) and (d) illustrate the origin of this failure from the carbon dimer potential energy landscape. Panel (c) shows that the potential energy $E(R) = V(R) - h(R) = (V_0(R) - h_0(R))f_C(R)$ drops more rapidly with dimer length R as the cutoff radius r_2 is decreased. The more rapid this drop, the larger the respective force shown in panel (d). The force required to break the dimer is the maximum of the force curve. The insets show the value (e) and derivative (f) of the cutoff function f_C. The cutoff function is unity below radius r_1 and drops to zero at r_2. The original REBO2 formulation uses r_2 = 2.0 Å (blue lines). Adapted from References 22 and 33. $V(R)$, repulsive potential; $h(R)$, bond integral; $V_0(R)$, asymptotic potential; and $h_0(R)$, asymptotic bond integral.

rediscovered for fracture of silicon.[36] However, such an approach has the disadvantage that the force-field becomes non-conservative, thus prohibiting the reforming of bonds.[37] These problems can be fixed by implementing an empirical screening function approach[33,38,39] to limit the interaction to the first-nearest neighbor shell while allowing the bond lengths to vary smoothly over a longer range. The idea behind this method is that two atoms interact as long as there is no third atom in the bonding area that screens the interaction.

This scheme was transferred[33] to Brenner's REBO2 to limit its interaction range using the screening function first published in Reference 38. Briefly, the bond integrals become $h_{ij} = h_0(R_{ij})S_{ij}$, where S_{ij} is a many-body term that accounts for the loss of bond strength due to the screening effect of neighboring atoms. Since this term depends on the ratios of distances only, the unphysical length scale, which is introduced in a distance-based cutoff formulation, is replaced by a scale-invariant ellipsoid with a fixed ratio of the axes' lengths. While this approach is completely empirical in nature, it leads to an overall functional form similar to environment-dependent screening functions used in orthogonal TB (OTB) formulations.[40,41]

Nguyen-Manh et al. rigorously showed that a non-orthogonal Hamiltonian can be reduced to an orthogonal Hamiltonian with such environment dependence,[42] giving a justification for using screening functions in related schemes.

The "screened" REBO2 formalism, which is referred to as REBO2+S in the following, corrects the fracture problem (see Figure 1b). Surprisingly, it also significantly improves the description of amorphous carbon (a-C) and hydrocarbon (a-C:H) phases. **Figure 2** shows how the hybridization (i.e., the fraction of sp^3 coordinated atoms) changes as a function of the density in the two amorphous carbon materials. This extensive comparison contains experimental data[43] together with theoretical predictions of accurate density functional theory (DFT) calculations,[44,45] a non-orthogonal density functional-based TB (DFTB) model,[46] orthogonal TB and related analytical bond order potentials that are discussed later in the text, the REBO potentials, and the purely empirical environmental-dependent interaction potential.[47] While the original REBO2 severely underestimates the sp^3 content for high densities, the improved REBO2+S closely reproduces the quantum calculations.

Bond breaking and making in carbon tribocontacts

The REBO2+S has enabled the study of crystalline and amorphous hydrocarbon systems under conditions where frequent bond-making and breaking events occur.[49–52] Such conditions are often encountered in tribological contacts, either when pressure and sliding velocity are large enough for the material to wear down, or if the surfaces are chemically active.

Severe wear is typical for machining processes that form one of the pillars of modern technology. Despite their significance, microscopic models for most industrial machining processes are largely lacking.[53] One example of such a process is the polishing of diamond wherein the hardest known material, usually exploited to machine other materials, is actually worn down. The particular process that is used to polish diamonds has remained unchanged for at least six centuries. Yet the microscopic details have remained a mystery. In this process, the polishing wheel is a cast iron disc (the scaife) with embedded diamond grit. The grit particles stick out of the iron surface and slide against the gemstone as the scaife rotates,[54] leading to diamond polishing of diamond.

The first scientific investigation of this process dates back to the work of Tolkowsky[55] in 1920. He concluded that the diamond gemstone fractures along low index planes, removing tiny chips of material. This explanation was later dismissed as high resolution microscopes became available and amorphous material was found beside[56,57] and later inside[58] the wear track.

Since diamond is pure carbon, it is an ideal candidate to be studied with the REBO potentials. Indeed, friction[59,60] and

https://doi.org/10.1557/mrs.2012.94 Published online by Cambridge University Press

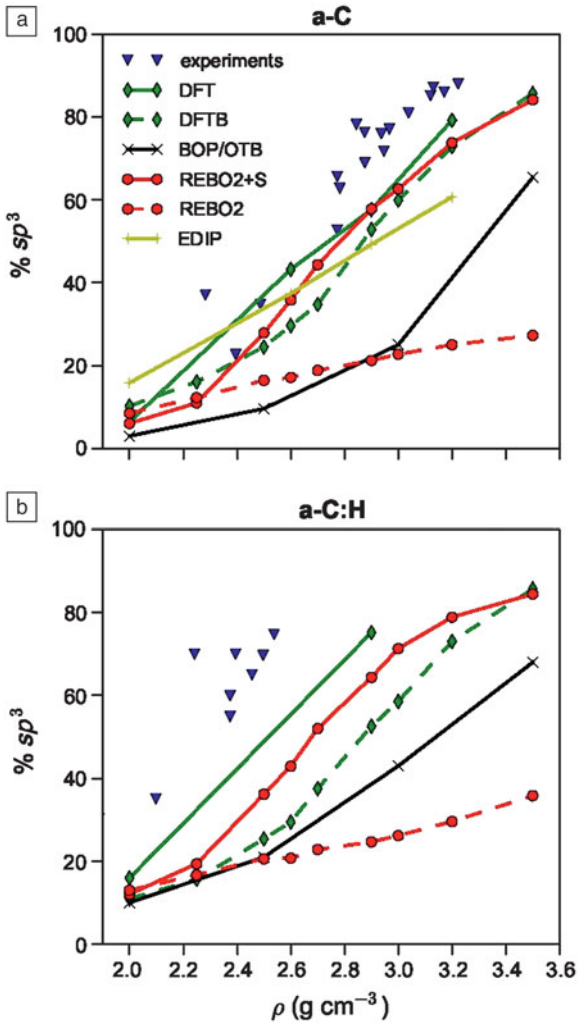


Figure 2. Hybridization (fraction of sp^3 carbon atoms) as a function of density for (a) a-C and (b) a-C:H for different quantum and classical methods. Experimental data are results from Reference 43, density functional theory data for a-C and a-C:H is taken from References 44 and 45, respectively, and environmental-dependent interaction potential (EDIP) data are taken from Reference 48. Note that experimental films are obtained from plasma enhanced physical vapor deposition processes, while the simulated samples are quenched from liquid carbon, resulting in slightly different hybridization.

mild wear situations[61] were studied shortly after the inception of REBO. In the unscreened formulation, the REBO, however, is unsuitable for the study of diamond machining where atoms are torn from the surface such that bonds repeatedly break and form. Hence REBO2+S was applied to model the severe conditions of diamond wear using a molecular dynamics simulation.[49]

In these simulations, it was initially assumed that tribochemical mechanisms, previously observed by Harrison and Brenner,[61] lead to a full dissociation of the surface termination. The residues of this process were modeled by a couple of adatoms placed between two pristine but unterminated diamond crystals that act as a seed for the destruction of the diamond. During sliding, pressure[50] and temperature[62] are controlled using specialized schemes that are designed for such tribosimulations. As sliding progresses, the system shears at the interface of the crystals, and each surface atom repeatedly forms and breaks bonds with continuously changing neighbors. A simple picture of this process is a layer of "pilot" atoms that move over the ordered phase, repeatedly pulling on the crystalline surface atoms. Since the amorphous environment of the "pilot" atoms changes over time, the pulling forces also change. A surface atom is then lifted into the amorphous phase when the pulling force happens to be larger than the force holding the surface atom to the crystal.

Surprisingly, different crystal orientations and sliding directions show different rates at which the atoms are lifted into the amorphous phase. **Figure 3** shows the pairing of the {110} surface in the soft <100> direction, which is known to show high wear rates, with the "harder" {100} surface in the <110> direction. The coloration in Figure 3 allows identification of the crystallite of origin for each atom. From this information, it becomes clear that atoms from the {110} surface turn more quickly into the amorphous phase than atoms from the {100} crystallite. Since such anisotropy is also experimentally found in the wear rate,[54,63] it was concluded that the formation of the amorphous layer is the rate limiting step in diamond polishing. This layer is then removed from the diamond surface by plowing or chemical etching with ambient O_2.[49,51,64]

These atomistic simulations have allowed unprecedented insights into the microscopic processes that take place. The inset in Figure 3 shows the progression of the atomic configuration on the {110} surface. As the "pilot" atoms move over the surface, the cyan 6-ring flips upright and is then subsequently integrated into the amorphous phase pulling along the following green and blue rows of atoms. This cascaded process is the reason why the amorphization is fastest on the {110} surface while sliding along the ⟨100⟩ direction. Since the reverse process is kinetically hindered, the amorphous phase grows, as shown in Figure 3. From this observation, a microscopic wear model based on the yield force to break C–C bonds can be derived.[49]

In a related example, REBO2+S was employed to study the frictional behavior of an amorphous hydrocarbon film,[50,52] which is widely used for low-friction wear-resistant coatings.[65] Surfaces that are "fresh," in that they have not yet experienced any tribological loading, show a decrease in friction coefficient during the initial frictional cycles that is known as "running-in" (**Figure 4**). An initially high friction coefficient (>0.1) drops over a few frictional cycles until it reaches a value as low as 0.01[66] or even 0.001.[67] The mechanisms of this initial running-in are also poorly understood, although changes in topography due to plastic deformation have been proposed.[67]

In reproducing experimental conditions as closely as possible, these surfaces were initially grown in a simulated vapor deposition process. Two such surfaces were then paired and slid under boundary conditions similar to the diamond case. Contrary to diamond polishing, interest here lay in the behavior

https://doi.org/10.1557/mrs.2012.94 Published online by Cambridge University Press

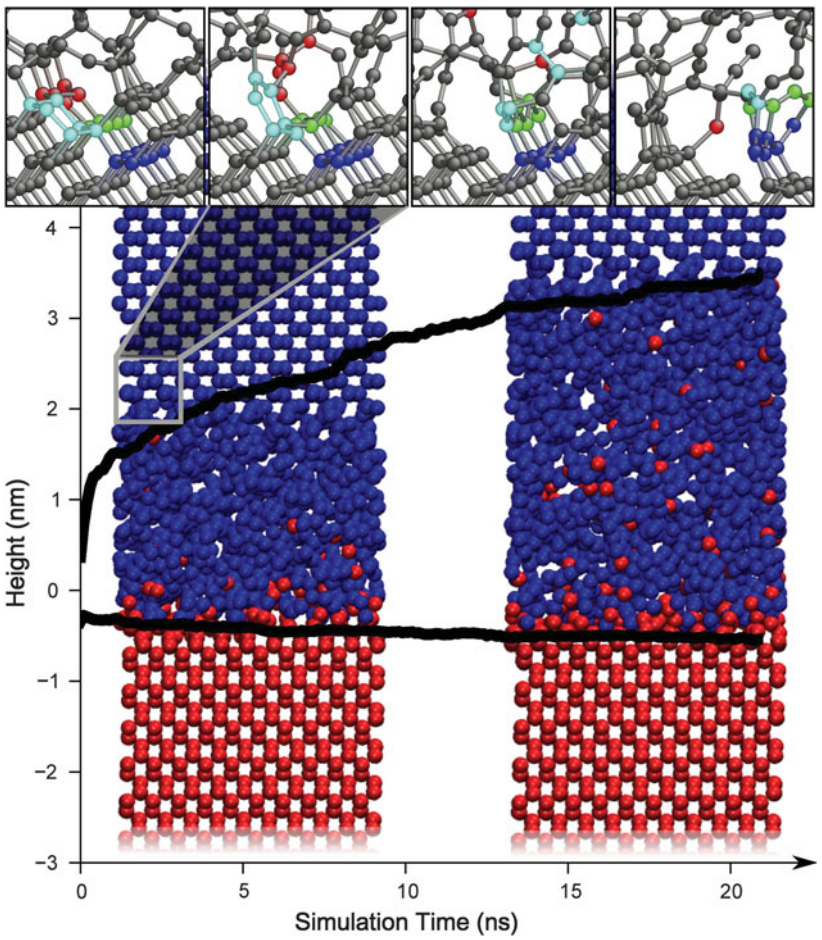


Figure 3. A {110} diamond crystallite sliding at 20 m s^{-1} in the ⟨100⟩ direction (blue) against a {100} crystallite oriented along the ⟨110⟩ axis in the sliding direction (red). Colors indicate whether an atom was bound to the top or bottom crystallite initially. The {110} surface, which is known to show lower wear than the {100} surface, shows a lower rate of amorphization. Black solid lines show the position of the amorphous interface over the course of 20 ns. The snapshots shown are taken at 5 ns (left) and 17.5 ns (right), respectively. Insets show snapshots of the microscopic details of the wear process on the {110} surface. At the beginning of the simulation (time zero), the interface between the two crystallites is located at zero height. Adapted from Reference 49.

of the friction coefficient, shown in Figure 4a for a sample with 30 at.% H. Clearly, the friction coefficient fluctuates dramatically in the initial stages and saturates over the period of 45 ns shown. The coefficient correlates with a measure of chemical bonding between the surfaces, shown in Figure 4b. As the system is in a steady state (run-in) and the friction coefficient is low, no further chemical bond linking the top to the bottom surface is observed. The passivation mechanism at work here is similar to the amorphization process described previously. As the red atom in the upper surface in Figure 4c moves, it repeatedly forms and breaks chemical bonds with various substrate atoms. When it approaches the blue atom in the lower surface, which has the "pilot" function here, the bond that forms (Figure 4d) is stronger than the bond holding the red atom to the top surface, such that the atom is transferred from the top to the bottom surface as sliding progresses. Now the red atom is bound to the lower surface (Figure 4e), where it eventually fully binds by saturating its dangling bonds (Figure 4f).

The dynamics of the breaking and making of chemical bonds at the interface is hence crucial for understanding the fundamental processes in friction and wear, requiring by its very nature a chemically accurate interatomic potential. Since most potentials are fitted to ground-state properties, they naturally provide a proper description for configurations not far from equilibrium. However, in the two previous examples, it is the balance of forces between the "pilot" surface atom and the substrate atoms that needs to be correct. This also requires a fair description of the slopes of the interatomic potential energy landscape. The screening function approach corrects this behavior in the REBO potential. No adjustment of the original potential parameters is required after the screening functions are introduced, which shows that the correct asymptotics of the functions describing bond integrals and repulsive potential are obtained from these ground-state fits already. Indeed, Brenner and co-workers hinted at the unphysical nature of the cut-off function when describing their second-generation REBO and noted that "other more complicated schemes will be needed, perhaps including self-consistent bonding concepts"[22] to exploit the full potential of the model.

Coarse graining the electronic structure: Rigorous derivation of the bond order expansions

While the empirical ATB potentials have proven successful in many applications, they were also found to suffer from some fundamental limitations such as overbinding of radicals due to the inability to describe dangling bonds, poor treatment of π and conjugated bonds, and sometimes incorrect differentiation of bulk structures. As described previously, some of these shortcomings have been corrected in subsequent generations or parameterizations of the ATB potentials. However, those related to the empirical nature of the models (i.e., inappropriate functional forms or missing contributions) are sometimes difficult or even impossible to cure.

As stated in the introduction, it is possible to derive the functional form of a many-body interatomic potential directly from the rigorous quantum mechanics of the electrons. The first cornerstone for such a rigorous derivation was laid in the late 1960s by Cyrot-Lackman[68] and Ducastelle[69] who showed that within the TB framework, a connection exists between the moments of the local density of states (LDOS) on an atom and the topology of the lattice in terms of self-returning hopping

https://doi.org/10.1557/mrs.2012.94 Published online by Cambridge University Press

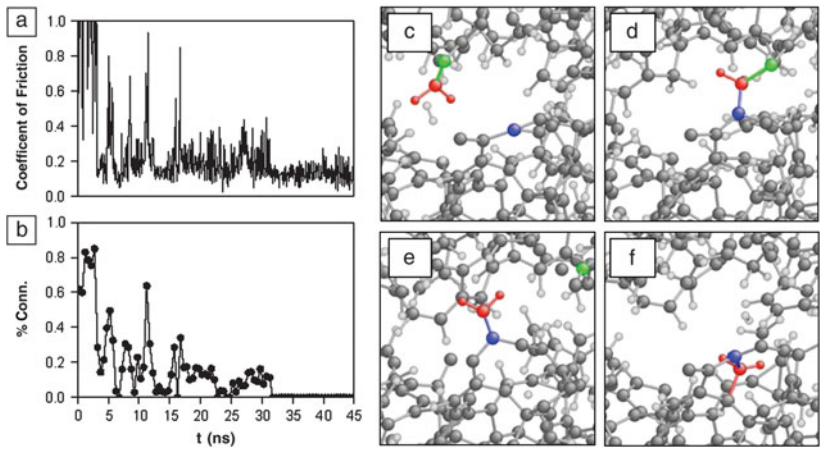


Figure 4. (a) Friction coefficient of two a-C:H surfaces with 30 at.% H sliding at 20 m s^{-1} and 1 GPa normal pressure. (b) Connectivity, defined as the relative amount of time a chemical bond exists between two surfaces over periods of 0.5 ns. (c)–(f) Snapshots of a typical passivation event that leads to a reduction in connectivity involving bond-breaking and formation processes. (c) The methylene group (red atoms) bound to the upper surface (green atom) binds to the lower sliding surface (blue atom) in panel (d). Movement of the upper surface strains the carbon-carbon bonds that connect the methylene to the top and bottom surfaces. The weaker bond to the top surface finally breaks (e) and, subsequently, the methylene finds a binding position (f) within the bulk of the bottom surface leading to passivation. In panels (c) to (f), carbon atoms are displayed by large gray spheres, while hydrogens are smaller white spheres. Adapted from Reference 50.

or bonding paths starting on the same atom (see **Figure 5**).[2,3] This crucial link between the electronic and atomistic modeling hierarchies can be formally written as

$$\mu_{i\alpha}^{(p)} = \int E^p D_{i\alpha}(E)\,dE = \left\langle i\alpha \middle| \hat{H}^p \middle| i\alpha \right\rangle, \quad (8)$$

where the pth moment, $\mu_{i\alpha}^{(p)}$, of the local density of states $D_{i\alpha}(E)$ equals the pth moment of the Hamiltonian projected on the same orbital $i\alpha$. The process of hopping on the lattice along closed paths of length p becomes more obvious when the previous equation is rewritten as

$$\mu_{i\alpha}^{(p)} = \sum_{j_1\beta_1 \cdots j_{p-1}\beta_{p-1}} H_{i\alpha,j_1\beta_1} H_{j_1\beta_1,j_2\beta_2} \cdots H_{j_{p-1}\beta_{p-1},i\alpha}, \quad (9)$$

with $H_{i\alpha,j\beta}$ describing the hop between orbitals $|i\alpha\rangle$ and $|j\beta\rangle$. The first moment consists of hops on a single site, the second of hops to the nearest neighbors and back, and so on. The more hops that are considered, the better the description of the LDOS obtained. Important here is that only moments higher than two provide information about the shape of the eigenspectrum. The simplest second-moment models, which sample the shells of nearest neighbors only, therefore can describe correctly the basic energetics associated with the electron occupation, but they cannot predict any properties related to the more subtle details of the electronic structure, for instance, the structural trends.[2,3]

The second major breakthrough came in 1989,[70] when Pettifor showed that the bond order can be written as a multi-atom expansion that depends not only on the self-returning hopping paths but also on the interference paths linking atoms i and j (see Figure 5). This fundamental development enabled derivation of explicit expressions for the bond order using a continued fraction expansion of the Green's function matrix elements, and hence paved the way for a controlled and systematic construction of rigorous bond order potentials (BOPs). In the last 20 years, several BOP implementations have been developed for both metallic and covalent materials.[71–73] These schemes mainly differ in the mathematical formalism of how the BOP expansion is carried out and truncated, depending on the bonding character of the material. Detailed presentations of these developments can be found in the original literature[70,71,74,75] and several recent books and reviews.[2,3,73]

In the present article, we want to briefly outline the analytic BOPs for *sp* valent systems,[76–80] since they can be considered to be counterparts to the empirical ATB potentials. The analytic BOPs for hydrocarbons, developed by Pettifor and Oleinik about 10 years ago,[76–78] contain the first theoretically derived expressions for both the σ and π bond orders, as well as the promotion energy. The analytic formula for the σ

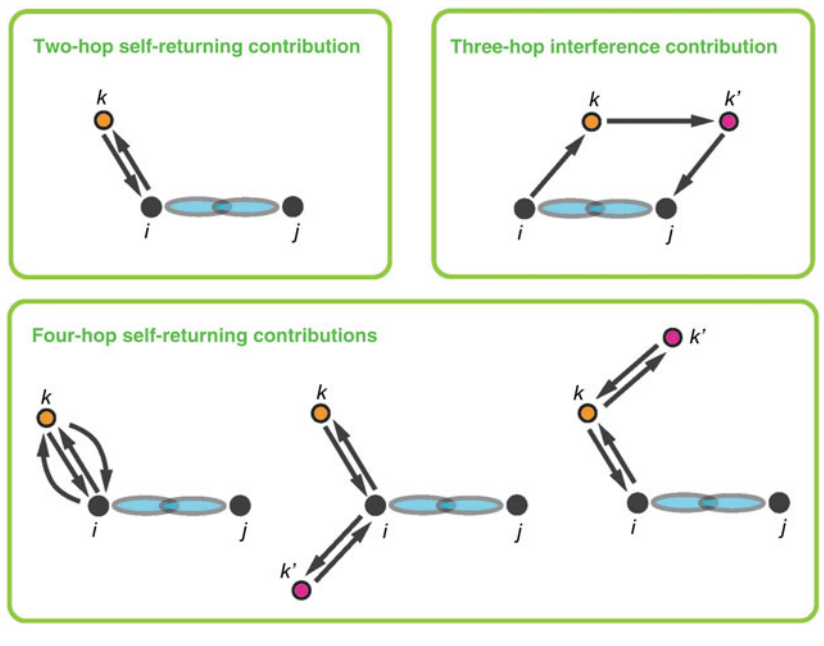


Figure 5. A schematic diagram of hopping paths included in the fourth-moment expansion of the bond order. The bond order between atoms i and j depends on the two-, three-, and four-hop contributions to the neighboring atoms k and k'.[76,80]

https://doi.org/10.1557/mrs.2012.94 Published online by Cambridge University Press

bond was obtained within the so-called symmetric four-level approximation as a function of two- and four-hop self-returning and three-hop interference contributions (see Figure 5). Interestingly, the second-moment term in the expansion turned out to be very similar to Tersoff's empirical expression for the bond order, thereby providing insight and justification for the empirical ATB schemes.[75] However, it was also shown that the fourth-moment terms are essential for a reliable description of the σ bond orders in the whole range of carbon bonding environments, from molecules and open bulk phases to close-packed and amorphous structures, when compared to the exact TB results.[80,81] The explicit π bond description presents another major improvement over the ATB potentials since it naturally leads to a proper treatment of conjugacy and rotation barriers in double, triple, and conjugated carbon bonds without any empirical correction terms.[22]

In spite of their increased complexity, the analytic BOPs remain computationally efficient, as demonstrated in deposition simulations of amorphous carbon (a-C) and hydrogenated carbon (a-C:H) films.[80] These large-scale simulations present a stringent test, since they describe film growth under non-equilibrium conditions of plasma deposition where the local atomic structure of the films is determined by breaking, stretching, and twisting of bonds induced by the impacting molecules. The study has shown that the key properties of the growing films, such as the density and the sp^3 content, depend sensitively on the energy of deposited species. These results are in qualitative but not fully quantitative agreement with available experimental observations,[43] according to which the sp^3 content of highly dense a-C:H films exceeds 80% compared to about 60% obtained in the BOP simulations. A detailed analysis of the amorphous structures revealed[80] that the primary reason for this problem lies not in the approximations used during the derivations of the bond order expressions but rather in deficiencies of the underlying OTB parameterization.[82] As shown in Figure 2, both BOP and its underlying OTB model (their results are identical within the error limits) give a systematic underestimation of the sp^3/sp^2 ratio in amorphous carbon structures. Hence, the BOP models inherit not only the strengths but also the limitations of the TB parameterizations on which they are based. In order to shift from qualitative to fully quantitative predictions, the quality of the TB models is therefore of outmost importance.

BOPs for transition metals and their compounds

Despite the notion of the metallic bond being delocalized, the bonding in technologically important transition metals and their compounds is, to a great extent, controlled by the *d* electrons that remain tightly bound to the atoms and form strong unsaturated covalent bonds. The bond order concept within the TB formalism is therefore well applicable for the description of energetics in the transition metal systems.

In contrast to covalent materials, higher-order (typically >4) moment expansions are needed for transition metals in order to obtain a sufficiently detailed representation of the LDOS that guarantees the correct prediction of structural trends among close-packed metallic structures.[2] The reliable description of bonding is also crucial for reliable modeling of extended defects in these materials, since the angular character of the bonding often governs their structures and properties. Popular many-body potentials for metals based on the second-moment approximation to the density of states[15,37,83] (see the article by Foiles and Baskes in this issue) are known to fail in identifying subtle differences in properties of dislocation cores, grain boundaries, or surfaces in transition metals and their compounds.[84–86]

A number of BOPs for transition metals,[87–90] as well as transition metal compounds,[91] have been completed in the past decade. These potentials have been used extensively in studies of dislocation properties and their relation to macroscopic mechanical behavior.[87,88] The simulations provided valuable atomistic insights and thus helped to resolve several outstanding and often unexpected features of plastic deformation such as the non-Schmid behavior of 1/2 ⟨111⟩ screw dislocations in bcc metals,[92–95] the unusual brittleness of fcc iridium,[96] or the origins of channeled flow in lamellar intermetallic TiAl.[97] Recently, the original BOP formalism was also generalized to magnetic materials, and the first magnetic bond order potential for iron has been developed.[98] The description of magnetic effects is of crucial importance, since ferromagnetism plays a dominant role in determining the stability of Fe bulk phases. Due to a correct description of bonding and the inclusion of magnetic interactions within the Stoner model of itinerant magnetism, the magnetic BOP is able to distinguish between various bulk magnetic phases of Fe (see **Figure 6**) and to correctly account for the collapse of magnetic moments as the structures are compressed.[98] This state-of-the-art potential is currently employed in atomistic studies of dislocation core structures under applied

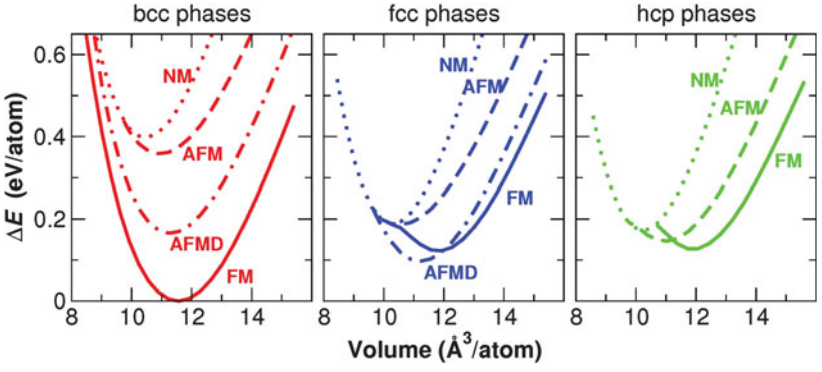


Figure 6. Relative stabilities of Fe bulk phases predicted by magnetic bond order potential. NM, non-magnetic; FM, ferromagnetic; AFM, anti-ferromagnetic; AFMD, anti-ferromagnetic double layer; bcc, body centered cubic; fcc, face centered cubic; hcp, hexagonal close packed; and ΔE is the energy difference.[98]

https://doi.org/10.1557/mrs.2012.94 Published online by Cambridge University Press

load, including the changes in local magnetic moments within the cores. Notwithstanding its quantum mechanical origin, the magnetic BOP is still computationally efficient to carry out large-scale simulations containing many thousands of atoms. This was demonstrated on studies of dislocation kinks that require fully 3D simulation blocks with large dimensions both perpendicular and parallel to the dislocation line.[98] **Figure 7** shows the predicted atomic structures of individual single kinks on the 1/2⟨111⟩ screw dislocation in α-Fe. These kinks are termed as vacancy and interstitial due to local tensile and compressive regions in their centers, though the number of atoms in both kinks is the same. According to the BOP simulations, the two kinks have clearly distinct atomic and magnetic structures.[98] Despite its denser core, the interstitial kink was found to have a lower formation energy than the more spacious vacancy kink. This somewhat surprising result is related to the magnetic effects since the central atoms of the interstitial kink prefer to flip their magnetic moments to an anti-ferromagnetic state to lower their energies. As shown by the superimposed lines in Figure 7, these factors also lead to much larger and inhomogeneous variations of the bond lengths in the center of the interstitial kink than in the case of the vacancy kink, where only marginal changes of the local magnetic moments were observed. Additionally, BOP simulations show that the kink region is rather compact, which is in contrast to simulations carried out with the classical second-moment potentials.[99] This result is most likely related to the central-force character of the potential that favors a conservation of atomic volumes rather than of bond angles.

The examples presented here demonstrate that BOPs for transition metals are a mature and full-featured scheme that can capture subtleties of chemical bonding and still be applied to studies of complex defect configurations in large atomic ensembles exceeding 10^5 atoms.

Summary and outlook

Many-body interatomic potentials based on the concept of the bond order are powerful tools for exploring the behavior of real materials. As we have described previously, simulations at the atomic scale can yield remarkable insights into experimentally inaccessible microscopic processes. In some situations, such "nanoscale" simulations can even help to explain macroscopic phenomena, such as plastic deformation or wear. For the bond order potentials to become even more useful for engineering purposes, the accessible length and time scales need to be further extended beyond the nm and ns, respectively, for instance, by incorporation into multiscale modeling schemes or by efficient implementation on massively parallel computers. As discussed by Plimpton and Thompson in this issue, higher computational cost—typical for bond order schemes—usually means higher parallel efficiency. Nevertheless, efficient parallel implementations of advanced bond order potentials, which involve multiple hopping paths to distant neighbors, will probably require more involved parallelization strategies than those used in the existing molecular dynamics codes.

Apart from these rather technical issues, probably the main scientific challenge that lies ahead is to cover a broader range of the periodic table, since most technologically important materials are compounds, alloys, or composite materials. Among the best examples are modern steels that have both complicated microstructure and chemistry. The bare minimum of elements needed for realistic steel simulations include Fe and C, several transition metals such as Cr, Mo, Mn, or Ni, and possibly also O, H, and other non-metallic elements.

Empirical potentials for multi-component systems, including those where significant charge transfer occurs, have been developed in recent years (see References 14, 100–102, and the article by Shin and co-workers in this issue). However, there is always a significant risk of failure when these models are applied to situations far from their proven fitting pools. For example, the charge transfer schemes employed in such multi-component potentials typically treat covalent systems as if they were metals.[102] This leads to a wrong scaling of polarizabilities with system size.[103] The number of possible cures, such as a modification of model parameters or an addition of further terms, is limited and becomes more difficult to apply the more complicated the models are.

Significant progress has been achieved with rigorous bond order potentials (BOPs) and tight-binding (TB) models, but their fitting may also be elaborate, in particular when multiple chemical elements need to be considered simultaneously. TB bond and overlap integrals can, in principle, be obtained directly from first-principles calculations by utilizing a suitable minimal basis of atomic orbitals. Several approaches have been proposed in the past,[46,104–106] and some of them[42,107,108] have been used for a systematic determination of TB and BOP parameterizations. The magnetic BOP for iron presented previously was parameterized using a novel projection scheme developed by Meyer and co-workers[109] that is based on simultaneous optimization and projection of atomic-like orbitals on

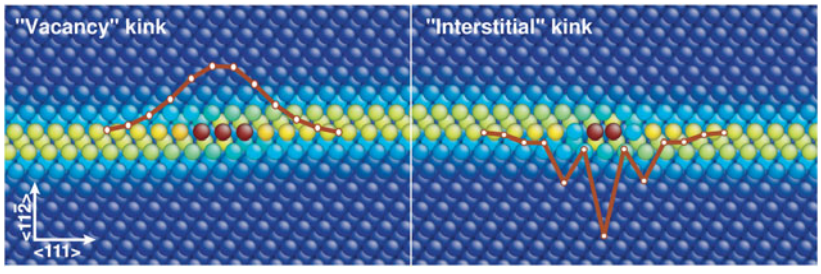


Figure 7. Atomic core structures of kinks on the 1/2 ⟨111⟩ screw dislocation in Fe. The coloring of atoms represents local distortions of atomic environment: the yellow atoms mark the dislocation core, and the red atoms are the kink core atoms. The superimposed curves show the relative increase and decrease of the nearest-neighbor bond lengths along the dislocation line in the vacancy and interstitial kinks, respectively.[98]

https://doi.org/10.1557/mrs.2012.94 Published online by Cambridge University Press

self-consistent density functional theory wave functions. The method is universally applicable to both elements and compounds and enables thorough testing of the transferability of TB parameters not only between different structural configurations but also in different chemical environments.[110]

We believe that such physically justified bottom-up approaches are indispensable for the construction of transferable models. Both sound and justifiable functional forms and transparent fitting strategies are crucial in particular for multicomponent systems where the number of model parameters explodes, and the fitting becomes very tedious and ambiguous. A typical sign of a lack of transferability in state-of-the-art interatomic potentials or even tight-binding models is the existence of separate parameter sets for an element under different conditions (e.g., liquid or solid phases) or for a binary system with different concentrations of its constituents. In situations where the complexity of atomic interactions prohibits the models to be both simple and accurate, the required accuracy could be reached by employing modern correction schemes, such as recent Gaussian approximation potentials,[111] instead of creating several specific parameterizations.

Potentials covering multiple elements and the whole spectrum of covalent, metallic, and polar chemical bonds still require further work. However, the theoretical groundwork laid and the experience gained in the last 30 years has clearly shown a rigorous route through which such a goal could be reached.

Acknowledgments

The authors acknowledge collaboration and many fruitful discussions with David Pettifor, Vasek Vitek, Christian Elsässer, Bernd Meyer, Duc Nguyen-Manh, Ralf Drautz, Jonathan Hird, and John Field. Financial support was provided by the German Research Foundation (DFG) via grants MR 22/5–1 and Gu 367/30, by the German Ministry of Education and Research (BMBF), Grants 03X0511 and 03X2512G, by the European Commission through contract No. NMP.2010.2.5–1.263335 (MultiHy), and a Marie-Curie fellowship for L.P. (IDOF 272619). Some simulations were carried out at the Jülich Supercomputing Center.

References

1. C. Coulson, *Proc. R. Soc. London, Ser. A* **169**, 413 (1939).
2. D.G. Pettifor, *Bonding and Structure of Molecules and Solids* (Oxford University Press, UK, 1995).
3. M.W. Finnis, *Interatomic Forces in Condensed Matter* (Oxford University Press, UK, 2004).
4. J. Slater, G. Koster, *Phys. Rev.* **94**, 1498 (1954).
5. G.C. Abell, *Phys. Rev. B* **31**, 6184 (1985).
6. J. Tersoff, *Phys. Rev. Lett.* **56**, 632 (1986).
7. J. Tersoff, *Phys. Rev. B* **39**, 5566 (1989).
8. J. Tersoff, *Phys. Rev. B* **38**, 9902 (1988).
9. J. Kioseoglou, P. Komninou, T. Karakostas, *Phys. Status Solidi B* **245**, 1118 (2008).
10. K. Matsunaga, C. Fisher, H. Matsubara, *Jpn. J. Appl. Phys.* **39**, 48 (2000).
11. K. Albe, *Comput. Mater. Sci.* **10**, 111 (1998).
12. K. Albe, W. Möller, K.-H. Heinig, *Radiat. Eff. Defects Solids* **141**, 85 (1997).
13. B. Ni, K.-H. Lee, S.B. Sinnott, *J. Phys. Condens. Matter* **16**, 7261 (2004).
14. K.O.E. Henriksson, K. Nordlund, *Phys. Rev. B* **79**, 144107 (2009).
15. M. Müller, P. Erhart, K. Albe, *J. Phys. Condens. Matter* **19**, 326220 (2007).
16. P. Erhart, K. Albe, *Phys. Rev. B* **71**, 035211 (2005).
17. N. Juslin, P. Erhart, P. Träskelin, J. Nord, K.O.E. Henriksson, K. Nordlund, E. Salonen, K. Albe, *J. Appl. Phys.* **98**, 123520 (2005).
18. T. Hammerschmidt, P. Kratzer, M. Scheffler, *Phys. Rev. B* **77**, 235303 (2008).
19. P. Erhart, N. Juslin, O. Goy, K. Nordlund, R. Müller, K. Albe, *J. Phys. Condens. Matter* **18**, 6585 (2006).
20. D.W. Brenner, *Phys. Rev. B* **46**, 1948 (1992).
21. D.W. Brenner, *Phys. Rev. B* **42**, 9458 (1990).
22. D.W. Brenner, O.A. Shenderova, J.A. Harrison, S.J. Stuart, B. Ni, S.B. Sinnott, *J. Phys. Condens. Matter* **14**, 783 (2002).
23. S.J. Stuart, A.B. Tutein, J.A. Harrison, *J. Chem. Phys.* **112**, 6472 (2000).
24. B.J. Garrison, E.J. Dawnkaski, D. Srivastava, D.W. Brenner, *Science* **255**, 835 (1992).
25. M. Eckert, E. Neyts, A. Bogaerts, *Cryst. Growth Des.* **10**, 3005 (2010).
26. M. Moseler, P. Gumbsch, C. Casiraghi, A.C. Ferrari, J. Robertson, *Science* **309**, 1545 (2005).
27. H.U. Jäger, K. Albe, *J. Appl. Phys.* **88**, 1129 (2000).
28. L. Pastewka, R. Salzer, A. Graff, F. Altmann, M. Moseler, *Nucl. Instrum. Methods Phys. Res., Sect. B* **267**, 3072 (2009).
29. P.T. Mikulski, L.A. Herman, J.A. Harrison, *Langmuir* **21**, 12197 (2005).
30. M. Buongiorno Nardelli, B.I. Yakobson, J. Bernholc, *Phys. Rev. Lett.* **81**, 4656 (1998).
31. M. Neek-Amal, F.M. Peeters, *Phys. Rev. B* **82**, 085432 (2010).
32. M. Marder, *Comput. Sci. Eng.* **1**(5), 48 (1999).
33. L. Pastewka, P. Pou, R. Pérez, P. Gumbsch, M. Moseler, *Phys. Rev. B* **78**, 161402(R) (2008).
34. P. Gumbsch, in *Materials Science for the 21st Century*, Y. Shibutani, S. Ogata, Eds. (The Society of Materials Science, JSMS, Japan, 2001), p. 50.
35. O.A. Shenderova, D.W. Brenner, A. Omeltchenko, X. Su, L.H. Yang, *Phys. Rev. B* **61**, 3877 (2000).
36. A. Mattoni, M. Ippolito, L. Colombo, *Phys. Rev. B* **76**, 224103 (2007).
37. M.S. Daw, M.I. Baskes, *Phys. Rev. B* **29**, 6443 (1984).
38. M.I. Baskes, J.E. Angelo, C.L. Bisson, *Modell. Simul. Mater. Sci. Eng.* **2**, 505 (1994).
39. M.I. Baskes, *Phys. Rev. B* **46**, 2727 (1992).
40. M.S. Tang, C.Z. Wang, C.T. Chan, K.M. Ho, *Phys. Rev. B* **53**, 979 (1996).
41. H. Haas, C.Z. Wang, M. Fähnle, C. Elsässer, K.M. Ho, *Phys. Rev. B* **57**, 1461 (1998).
42. D. Nguyen-Manh, D.G. Pettifor, V. Vitek, *Phys. Rev. Lett.* **85**, 4136 (2000).
43. A.C. Ferrari, A. Libassi, B.K. Tanner, V. Stolojan, J. Yuan, L.M. Brown, S.E. Rodil, B. Kleinsorge, J. Robertson, *Phys. Rev. B* **62**, 11089 (2000).
44. D.G. McCulloch, D.R. McKenzie, C.M. Goringe, *Phys. Rev. B* **61**, 2349 (2000).
45. M.M.M. Bilek, D.R. McKenzie, D.G. McCulloch, C.M. Goringe, *Phys. Rev. B* **62**, 3071 (2000).
46. D. Porezag, T. Frauenheim, T. Köhler, G. Seifert, R. Kaschner, *Phys. Rev. B* **51**, 12947 (1995).
47. N.A. Marks, *Phys. Rev. B* **63**, 035401 (2000).
48. N.A. Marks, *J. Phys. Condens. Matter* **14**, 2901 (2002).
49. L. Pastewka, S. Moser, P. Gumbsch, M. Moseler, *Nat. Mater.* **10**, 34 (2011).
50. L. Pastewka, S. Moser, M. Moseler, *Tribol. Lett.* **39**, 49 (2010).
51. G. Moras, L. Pastewka, P. Gumbsch, M. Moseler, *Tribol. Lett.* **44**, 355 (2011).
52. L. Pastewka, S. Moser, M. Moseler, B. Blug, S. Meier, T. Hollstein, P. Gumbsch, *Int. J. Mater. Res.* **99**, 1136 (2008).
53. H.C. Meng, K.C. Ludema, *Wear* **181–183**, 443 (1995).
54. J.R. Hird, J.E. Field, *Proc. R. Soc. London, Ser. A* **460**, 3547 (2004).
55. W. Tolkowsky, DSc degree thesis, City and Guilds College, University of London (1920).
56. F.M. van Bouwelen, A.L. Bleloch, J.E. Field, L.M. Brown, *Diamond Relat. Mater.* **5**, 654 (1996).
57. Z. Feng, J.E. Field, *J. Phys. D: Appl. Phys.* **25**, A33 (1992).
58. A.R. Konicek, D.S. Grierson, P.U.P.A. Gilbert, W.G. Sawyer, A.V. Sumant, R.W. Carpick, *Phys. Rev. Lett.* **100**, 235502 (2008).
59. S.B. Sinnott, S.-J. Heo, D.W. Brenner, J.A. Harrison, D.L. Irving, in *Nanotribology and Nanomechanics I*, B. Bhushan, Ed. (Springer, Berlin, Heidelberg, 2011), pp. 439–525.
60. J.A. Harrison, C.T. White, R.J. Colton, D.W. Brenner, *MRS Bull.* **18**, 50 (1993).
61. J.A. Harrison, D.W. Brenner, *J. Am. Chem. Soc.* **116**, 10399 (1994).
62. E.A.J.F. Peters, *Europhys. Lett.* **66**, 311 (2004).
63. B.S. El-Dasher, J. Gray, J. Tringe, J. Biener, A. Hamza, C. Wild, E. Worner, P. Koidl, *Appl. Phys. Lett.* **88**, 241915 (2006).
64. G. Moras, L. Pastewka, J. Schnagl, M. Walter, P. Gumbsch, M. Moseler, *J. Phys. Chem. C* **115**, 24653 (2011).
65. J. Robertson, *Mater. Sci. Eng. R* **37**, 129 (2002).
66. K. Enke, *Thin Solid Films* **80**, 227 (1981).
67. J. Fontaine, T. Le Mogne, J.L. Loubet, M. Belin, *Thin Solid Films* **482**, 99 (2005).
68. F. Cyrot-Lackmann, *Adv. Phys.* **16**, 393 (1967).
69. F. Ducastelle, F. Cyrot-Lackmann, *J. Phys. Chem. Solids* **31**, 1295 (1970).

https://doi.org/10.1557/mrs.2012.94 Published online by Cambridge University Press

70. D.G. Pettifor, *Phys. Rev. Lett.* **63**, 2480 (1989).
71. A.P. Horsfield, A.M. Bratkovsky, M. Fearn, D.G. Pettifor, M. Aoki, *Phys. Rev. B* **53**, 12694 (1996).
72. R. Drautz, D.G. Pettifor, *Phys. Rev. B* **74**, 174117 (2006).
73. M. Finnis, E.R. Drautz, *Prog. Mater. Sci.* **52**, 131 (2007).
74. D.G. Pettifor, M. Aoki, in *Structural and Phase Stability of Alloys*, J.L. Moran-Lopez, F. Mejia-Lira, J.M. Sanchez, Eds. (Plenum Press, New York, 1992), pp. 119–132.
75. P. Alinaghian, P. Gumbsch, A.J. Skinner, D.G. Pettifor, *J. Phys. Condens. Matter* **5**, 5795 (1993).
76. D.G. Pettifor, I.I. Oleinik, *Phys. Rev. B* **59**, 8487 (1999).
77. D.G. Pettifor, I.I. Oleinik, *Phys. Rev. Lett.* **84**, 4124 (2000).
78. D.G. Pettifor, I.I. Oleinik, *Phys. Rev. B* **65**, 172103 (2002).
79. B.A. Gillespie, X.W. Zhou, D.A. Murdick, H.N.G. Wadley, R. Drautz, D.G. Pettifor, *Phys. Rev. B* **75**, 155207 (2007).
80. M. Mrovec, M. Moseler, C. Elsässer, P. Gumbsch, *Prog. Mater. Sci.* **52**, 230 (2007).
81. I.I. Oleinik, D.G. Pettifor, *Phys. Rev. B* **59**, 8500 (1999).
82. C.H. Xu, C.Z. Wang, C.T. Chan, K.M. Ho, *J. Phys. Condens. Matter* **4**, 6047 (1992).
83. M.W. Finnis, J.E. Sinclair, *Philos. Mag. A* **50**, 45 (1984).
84. D.G. Pettifor, M. Aoki, P. Gumbsch, A.P. Horsfield, D. Nguyen-Manh, V. Vitek, *Mater. Sci. Eng., A* **192/193**, 24 (1995).
85. M. Mrovec, C. Elsasser, P. Gumbsch, *Philos. Mag.* **89**, 3179 (2009).
86. Z.M. Chen, M. Mrovec, P. Gumbsch, *Modell. Simul. Mater. Sci. Eng.* **19**, 074002 (2011).
87. M. Mrovec, D. Nguyen-Manh, D.G. Pettifor, V. Vitek, *Phys. Rev. B* **69**, 094115 (2004).
88. M. Mrovec, R. Gröger, A.G. Bailey, D. Nguyen-Manh, C. Elsässer, V. Vitek, *Phys. Rev. B* **75**, 104119 (2007).
89. M.J. Cawkwell, D. Nguyen-Manh, D.G. Pettifor, V. Vitek, *Phys. Rev. B* **73**, 064104 (2006).
90. A. Girshick, A.M. Bratkovsky, D.G. Pettifor, V. Vitek, *Philos. Mag. A* **77**, 981 (1998).
91. S. Znam, D. Nguyen-Manh, D.G. Pettifor, V. Vitek, *Philos. Mag. A* **83**, 415 (2003).
92. V. Vitek, M. Mrovec, R. Gröger, J. Bassani, V. Lacherla, L. Yin, *Mater. Sci. Eng., A* **387**, 138 (2004).
93. V. Vitek, M. Mrovec, J.L. Bassani, *Mater. Sci. Eng., A* **365**, 31 (2004).
94. R. Gröger, A.G. Bailey, V. Vitek, *Acta Mater.* **56**, 5401 (2008).
95. R. Gröger, V. Vitek, *Acta Mater.* **56**, 5426 (2008).
96. M.J. Cawkwell, D. Nguyen-Manh, C. Woodward, D.G. Pettifor, V. Vitek, *Science* **309**, 1059 (2005).
97. I.H. Katzarov, A.T. Paxton, *Phys. Rev. Lett.* **104**, 225502 (2010).
98. M. Mrovec, D. Nguyen-Manh, C. Elsässer, P. Gumbsch, *Phys. Rev. Lett.* **106**, 246402 (2011).
99. L. Ventelon, F. Willaime, P. Leyronnas, *J. Nucl. Mater.* **386**, 26 (2009).
100. P.T. Mikulski, M.T. Knippenberg, J.A. Harrison, *J. Chem. Phys.* **131**, 241105 (2009).
101. K. Albe, J. Nord, K. Nordlund, *Philos. Mag.* **89**, 3477 (2009).
102. T.-R. Shan, B.D. Devine, J.M. Hawkins, A. Asthagiri, S.R. Phillpot, S.B. Sinnott, *Phys. Rev. B* **82**, 235302 (2010).
103. T. Verstraelen, V. van Speybroeck, M. Waroquier, *J. Chem. Phys.* **131**, 044127 (2009).
104. O.K. Andersen, O. Jepsen, *Phys. Rev. Lett.* **53**, 2571 (1984).
105. W.C. Lu, C.Z. Wang, T.L. Chan, K. Ruedenberg, K.M. Ho, *Phys. Rev. B* **70**, 041100 (2004).
106. X. Qian, L. Ju, L. Qi, C. Wang, T. Chan, Y. Yao, K. Ho, S. Yip, *Phys. Rev. B* **78**, 245112 (2008).
107. D. Nguyen-Manh, D.G. Pettifor, D.J.H. Cockayne, M. Mrovec, S. Znam, V. Vitek, *Bull. Mater. Sci.* **26**, 43 (2003).
108. D. Nguyen-Manh, V. Vitek, A.P. Horsfield, *Prog. Mater. Sci.* **52**, 255 (2007).
109. A. Urban, M. Reese, M. Mrovec, C. Elsässer, B. Meyer, *Phys. Rev. B* **84**, 155119 (2011).
110. E.R. Margine, A.N. Kolmogorov, M. Reese, M. Mrovec, C. Elsässer, B. Meyer, R. Drautz, D.G. Pettifor, *Phys. Rev. B* **84**, 155120 (2011).
111. A.P. Bartók, M.C. Payne, R. Kondor, G. Csányi, *Phys. Rev. Lett.* **104**, 136403 (2010). □

2GCMEA

2nd Global Congress on Microwave Energy Applications

July 23-27, 2012 ▪ Hilton Long Beach ▪ Long Beach, California, USA



REGISTER BY JULY 11, 2012 AND SAVE!

Join us for the only microwave conference of 2012! The **2nd Global Congress on Microwave Energy Applications (2GCMEA 2012)**, hosted in beautiful Long Beach, California, will feature plenary sessions, parallel topical sessions, poster sessions, an industrial exhibition and short courses. The Conference Banquet will be held aboard the historic Queen Mary, the iconic floating museum. Banquet tickets may be purchased with registration. Mark your calendar today and plan to attend 2GCMEA 2012, where the theme is "EM Solutions for Our Changing World."

The five-day conference will concentrate on the following four topical categories:

- **Energy/Environment**
  Sessions focus on how microwave and RF energy can have an impact on the global environment by creating a greener process, shorter times, waste minimization, process energy devices, energy storage devices and recycling.
- **Microwaves in Every Day Life**
  Sessions focus on the impact of microwave/RF energy in our daily lives. Topics include new material processes for polymers, ceramics, metals, transportation, construction, biological, modeling of processes and dielectric data.
- **Chemistry and Medicine**
  Sessions focus on microwave/material interactions, material synthesis, nanotechnology, microwave in the medical/dental fields, cell growth, drug delivery and meta-materials.
- **Manufacturing, Equipment and Process Control**
  Sessions focus on equipment, measurements, process control, applications (commercial, industrial and research) and modeling.

For the most up-to-date information on 2GCMEA 2012, including the complete list of program topics, hotel information, short courses and more, visit www.mrs.org/2gcmea-2012.

https://doi.org/10.1557/mrs.2012.94 Published online by Cambridge University Press